THE ASTROPHYSICAL JOURNAL, 429:233–240, 1994 July 1

A MULTIWAVELENGTH STUDY OF IRAS 19550+3248: A PROTOSTAR POSSIBLY FORMED BY A CLOUD-CLOUD COLLISION[1]

BON-CHUL KOO,[2,3] YOUNGUNG LEE,[4,5] G. A. FULLER,[3,5] MYUNG GYOON LEE,[2,6] SUK-MINN KWON,[7] AND JAE-HOON JUNG[8]

Received 1993 August 31; accepted 1993 December 22

ABSTRACT

We have carried out radio, near-infrared, and optical observations of the *IRAS* point source IRAS 19550+3248. ^{12}CO $J = 1$–0 line observations revealed a high-velocity (HV) molecular outflow centered on IRAS 19550+3248. The HV gas has a bipolar pattern with the blue and red peaks separated by 1′ along the north-south direction. The mechanical luminosity of the HV molecular outflow is $\sim 9 \times 10^{31} d_2$ ergs s^{-1}, and its dynamical age is $\sim 5 \times 10^4 d_2$ yr, where d_2 is the distance to the source normalized to 2 kpc. Inside the 95% confidence ellipse of *IRAS* position, we have detected a nebulous K band source. The nebulosity extends to $0.1 d_2$ pc in the east-west direction. In R and I bands, the source appears to be composed of two extended weak peaks shifted toward the blueshifted CO lobe from the peak position in K band. These near-infrared emission features are likely scattered stellar light. The infrared source has a steep spectral index between 2 and 25 μm ($d \log [\nu F_\nu]/d \log \nu = -0.93$), which indicates that it is a protostar deeply embedded in a dense molecular cloud core. The bolometric luminosity based on R, I, H, and K band photometry together with the *IRAS* data is $150 d_2^2\ L_\odot$.

IRAS 19550+3248 is located at the center of a small (4′ × 7′) dense molecular clump. The clump is at the tip of a long ($\sim 1°$) filamentary molecular cloud. The molecular cloud is composed of clumps which are not confined by gravity and nor, probably, by external pressure. The characteristic timescale for dispersal is $\sim 6 \times 10^6$ yr. We suggest cloud-cloud collision as a possible mechanism for the disruption of the cloud and for the formation of IRAS 19550+3248.

Subject headings: infrared: ISM: continuum — ISM: clouds — ISM: individual (IRAS 19550+3248) — ISM: molecules — radio lines: ISM — stars: formation

1. INTRODUCTION

Star formation appears either to proceed spontaneously or to be induced by some external perturbations. In a scenario of "spontaneous" star formation, self-gravitating, magnetically supported molecular clouds develop dense cores of sizes less than 0.1 pc, a characteristic size below which ambipolar diffusion is so effective that neutral particles do not experience restoring magnetic forces (Mouschovias 1987). These cores, either quasi-statically or dynamically, contract to reach the supercritical mass-to-flux ratio and undergo inside-out collapse to form low-mass stars (Shu, Adams, & Lizano 1987; Mouschovias & Morton 1992a, b, and references therein). The above scenario may be applicable to the formation of low-mass stellar associations in dark cloud complexes such as the Taurus complex (cf. Gomez de Castro & Pudritz 1992), or to the formation of a single (or multiple) low-mass star(s) in an isolated small globule such as B335 (Zhou et al. 1990). Formation of high-mass stars, on the other hand, has been speculated to be induced by external shocks. The spatially and temporally ordered subgroups in nearby stellar associations suggest that the star formation has been induced by the ionization-driven shocks, supernovae shocks, and stellar winds from a previous generation of OB stars (Lada, Blitz, & Elmegreen 1978; Blaauw 1991, and references therein). Star formation induced by a cloud-cloud collision has also been proposed (Loren 1976). Analytical and numerical studies have shown that, depending on various physical parameters of the colliding clouds, star formation can be triggered by a cloud-cloud collision (e.g., Hausman 1981; Gilden 1984; Lattanzio et al. 1985; Habe & Ohtka 1992).

In this paper, we report the discovery of a protostellar object formed at the tip of a long ($\sim 1°$) filamentary molecular cloud. The distance to the object is uncertain. If we use the kinematic distance 2 kpc to the cloud, the luminosity of the protostellar object is $\sim 150\ L_\odot$. The mass of the filamentary cloud is $\sim 2100\ M_\odot$ (Koo et al. 1993, hereafter KYHL). There is no evidence for other luminous protostellar objects in the cloud. Formation of a single (or multiple) star(s) at the tip of a large filamentary cloud does not seem to be consistent with the scenario of spontaneous star formation. We suggest that the formation of the protostellar object was possibly triggered by a cloud-cloud collision. The discovery of the protostellar object was made by its CO bipolar outflow. We carried out molecular line observations toward the bipolar outflow source, and the results are summarized in § 3. Located at the center of the bipolar outflow is the *IRAS* point source IRAS 19550+3248. We carried out near-infrared and optical imaging of IRAS

[1] Based in part on observations made at Palomar Observatory, which is owned and operated by the California Institute of Technology (Caltech). The Palomar 1.5 m telescope is jointly owned by Caltech and the Carnegie Observatories.

[2] Department of Astronomy, Seoul National University, Seoul 151-742, Korea.

[3] Also Harvard-Smithsonian Center for Astrophysics.

[4] Five College Radio Astronomy Observatory, University of Massachusetts. Current address: Department of Astronomy, University of Florida, Gainesville, FL 32611.

[5] National Radio Astronomy Observatory, 949 North Cherry Avenue, Campus Building 65, Tucson, AZ 85721-0665.

[6] Also The Observatories of the Carnegie Institution of Washington.

[7] Department of Science Education, Kangwon National University, Chun-Cheon 200-701, Korea.

[8] Daeduk Radio Astronomy Observatory, Daejun 305-348, Korea.

19550+3248, and the results are summarized in § 4. In § 5, we discuss some dynamical properties of the filamentary molecular cloud and suggest a possible scenario for the formation of IRAS 19550+3248. In § 6, we summarize our main results.

2. OBSERVATIONS

Molecular line observations were made using the 14 m telescope (FWHM = 45″ at 115 GHz) at the Five College Radio Astronomy Observatory (FCRAO)[9] in 1991 October and November. The 15 beam receiver QUARRY was used with two 32 channel filterbanks, one with 250 kHz and the other with 1 MHz frequency resolution and spacing. The 8′.3 × 5′ area centered at $(\alpha_{1950}, \delta_{1950}) = (19^h54^m59^s.4, +32°48'21'')$ was mapped at 50″ spacing in ^{12}CO $J = 1$–0 (115.2712 GHz). The central position was also observed in ^{13}CO $J = 1$–0 (110.20137 GHz), HCO^+ $J = 1$–0 (89.18852 GHz), and CS $J = 2$–1 (97.98101 GHz) lines. Additional ^{13}CO $J = 1$–0 line observations with high-frequency resolution were made using the 14 m telescope at Daeduk Radio Astronomy Observatory in 1993 Feburary. Typical system temperature was 700 K. The Daeduk telescope is located at 110 m above sea level in Daeduk, Korea (127°.4E, 36°.4N). The telescope is inside a radome and has a beam efficiency of 0.45 at 110 GHz. A 1024 channel autocorrelator was used with a bandwidth of 20.48 MHz. Three positions centered at IRAS 19550+3248, $(\alpha_{1950}, \delta_{1950}) = (19^h55^m00^s.0, +32°48'28'')$, were observed.

The near-infrared observations of IRAS 19550+3248 were made on 1992 June 17 and 22 using the IR Imager (IRIM), which contains a 58 × 62 (45″ × 48″) InSb array on the 2.1 m telescope of the National Optical Astronomy Observatories (NOAO)[10] at Kitt Peak. On both nights, a 3 × 3 mosaic was made around the *IRAS* position of IRAS 19550+3248. On June 17, the center-to-center distance for the mosaic was 10″, while on June 22, a 30″ spacing was used in order to cover a larger region. On each night, both H (1.65 μm) and K (2.16 μm) bands were observed, and each position in the mosaic was observed for 30 s in each filter. The seeing was about 1″.8. The observations were calibrated against standard stars observed before and after observing the source each night. We estimate that the uncertainty in both H and K magnitudes is about ±0.1 mag.

The optical (V, R, and I) observations of IRAS 19550+3248 were made on 1992 June 27 and 28 using a thinned Tektronix 1024 × 1024 (6′.3 × 6′.3) CCD camera on the Palomar 1.5 m telescope. The exposure times were 180, 120, and 80 s for V, R, and I, respectively. Seeing ranged from 1″.3 to 1″.7. The instrumental magnitudes of stars, obtained using the digital software DoPHOT (Schechtor, Mateo, & Saha 1993), were then calibrated onto the VRI standard system using the standard stars (Landolt 1992) observed on the same night.

3. RESULTS OF MOLECULAR LINE OBSERVATIONS

3.1. *Bipolar Molecular Outflow*

Figure 1 shows three ^{12}CO spectra (*solid lines*) along the north-south direction across IRAS 19550+3248. The spectrum at the central position clearly has a symmetric broad wing extending from +8 to +18 km s^{-1} in addition to a narrow ($\Delta v_{FWHM} = 2.7$ km s^{-1}) peak centered at +12.3 km s^{-1}. The northern and the southern CO spectra, on the other hand, have mainly a blueshifted wing and a redshifted wing, respectively. The high-velocity (HV) wing is not seen in the corresponding ^{13}CO spectra (*dotted lines*). If we take a flat rotation curve with $R_\odot = 8.5$ kpc and $v_\odot = 220$ km s^{-1}, the central velocity of the CO line, +12.3 km s^{-1}, implies a kinematic distance of 2.0 kpc (at $l = 69°.3$). We adopt $d = 2d_2$ kpc as the distance to the source.

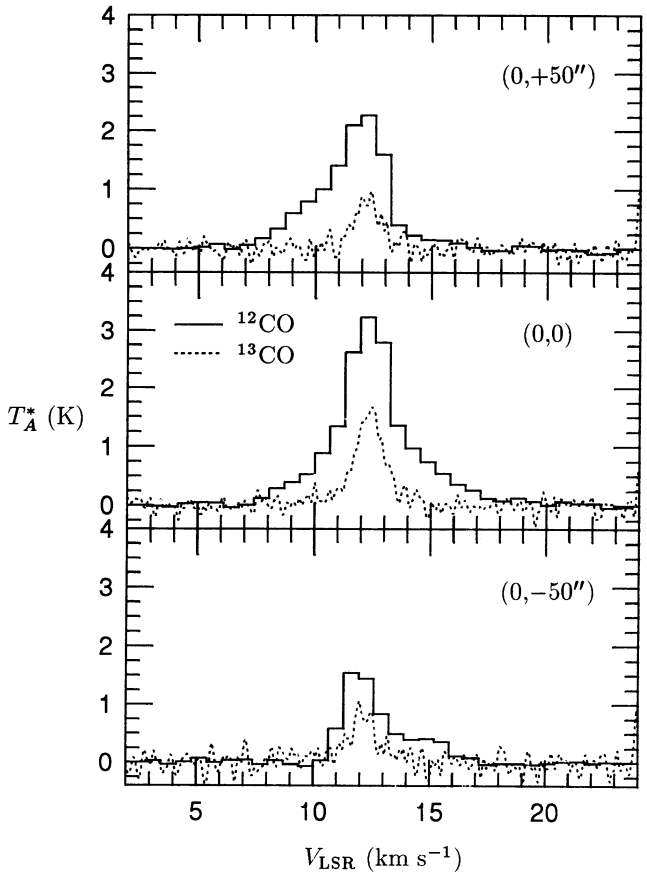

FIG. 1.—Three ^{12}CO (*solid lines*) and ^{13}CO (*dotted lines*) spectra along the north-south direction across IRAS 19550+3248.

The distribution of the HV gas is shown in Figure 2, together with the distribution of the low velocity gas. Figure 2 shows that the HV gas is centered on IRAS 19550+3248, which is located in the core of a small (4′ × 7′) dense clump. The HV gas has a bipolar pattern with the blue and red peaks separated by 1′ along the north-south direction. The structure of the HV molecular outflow is not resolved in our observation.

The mass of the HV gas is estimated by assuming that the ^{12}CO line is optically thin and is in local thermodynamic equilibrium (LTE) at $T_{ex} = 8$ K, which is the excitation temperature of the low-velocity gas (see § 3.2). The comparison of the ^{12}CO and ^{13}CO spectra at the central position, obtained by the same FCRAO telescope, shows that $T_A^*(^{12}\text{CO})/T_A^*(^{13}\text{CO}) \sim 40$ at $v_{LSR} = +14.9$ km s^{-1}, which suggests that the ^{12}CO emission is optically thin in the HV wings. If we assume the abundance ratio $[H_2]/[CO] = 1 \times 10^4$, the masses of the blueshifted and the redshifted HV molecular gas (including helium with [He]/[H] = 0.1) are $0.14 \pm 0.04 d_2^2$ $M_\odot$ and $0.21 \pm 0.03 d_2^2$ $M_\odot$, respectively. If we further assume that the HV gas is moving at

[9] FCRAO is operated with support from the National Science Foundation and with the permission of the Metropolitan District Commission of the Commonwealth of Massachusetts.

[10] The NOAO is operated by Associated Universities, Inc., under contract with the National Science Foundation.

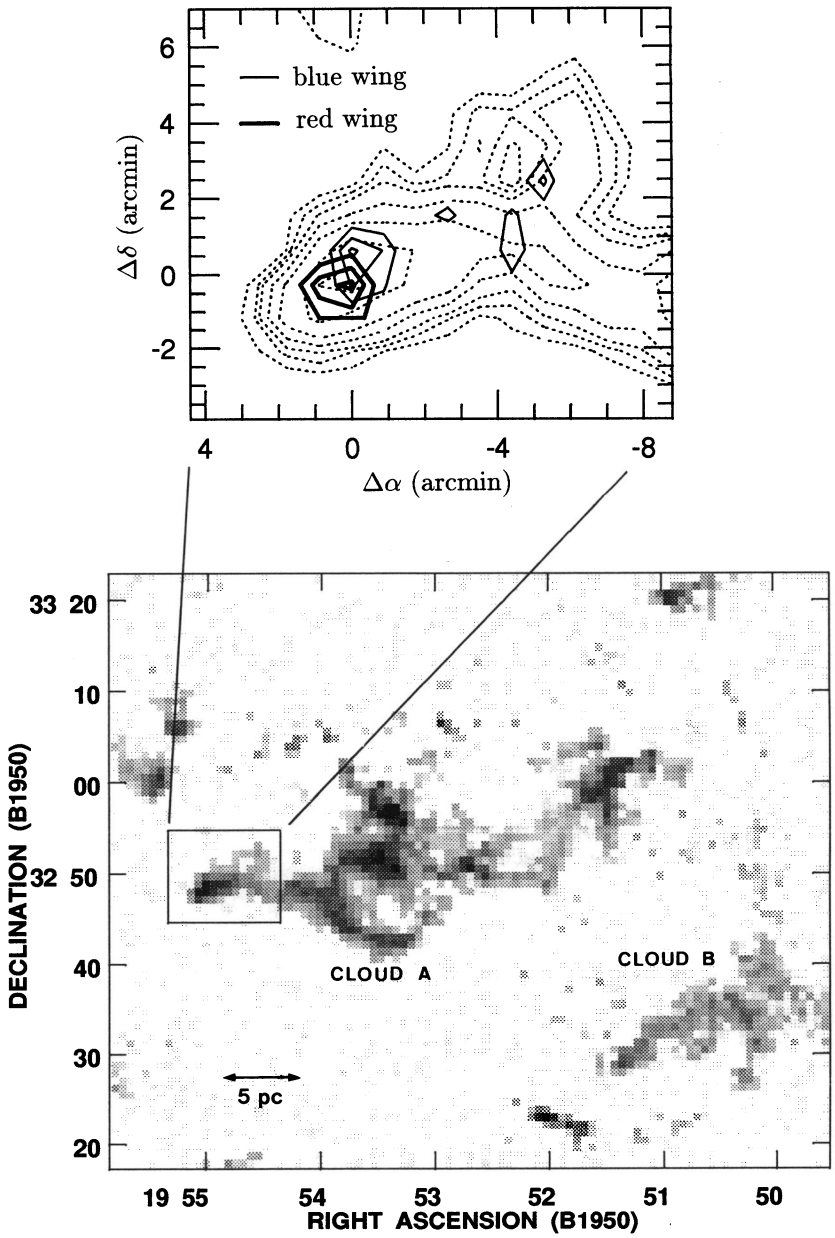

FIG. 2.—*Top*: Distribution of the HV gas (*solid lines*) together with the low-velocity gas (*dotted lines*). The coordinates are relative to IRAS 19550+3248. The blue wing is integrated between +5.5 and +10.0 km s^{-1}, and the red wing between +14.6 and +20.4 km s^{-1}. The contour intervals (in K km s^{-1}) are $\int T_A\,dv$ = 0.4, 0.8, 1.2, 2, 3, 5, and 7. *Bottom*: A large-scale map showing the distribution of the total integrated CO J = 1–0 intensity in this region (see KYHL). In KYHL, the cloud with a complicated structure near the central field of the map is called "cloud A" and the cloud located at the southwest is called "cloud B."

v_s = 6 km s^{-1}, the momentum and the kinetic energy of the HV gas are $2.2 \pm 0.4 d_2^2$ $M_\odot$ km s^{-1} and $1.3 \pm 0.3 \times 10^{44} d_2^2$ ergs, respectively. If we take 1′ (=$0.58 d_2$ pc) as the characteristic radius R_s of the flow, then the dynamical age of the flow is $R_s/2v_s \sim 4.7 \times 10^4 d_2$ yr. The derived physical parameters of the HV flow are summarized in Table 1.

3.2. *Molecular Clump and Virial Equilibrium*

The mass of the molecular clump, within which the bipolar outflow source is located, is estimated in two ways. First, since the ^{12}CO line at the central position is optically thick, the excitation temperature is T_{ex} = 8 K (using the main-beam efficiency of 0.7). By assuming LTE, the comparison of the ^{12}CO and the ^{13}CO spectra at the central position yields the optical depth of the ^{13}CO line at each velocity interval, which ranges from 0.2 to 0.9. If we use the abundance ratios [^{12}CO]/[^{13}CO] = 50 and [H_2]/[CO] = 1 × 10^4, the molecular hydrogen column density becomes 2.8 × 10^{21} cm^{-2}. If we assume that the clump is roughly spherical with a diameter of 5′ (=$2.9 d_2$ pc), then the mean density of the molecular hydrogen is $310 d_2^{-1}$ cm^{-3} and the total hydrogen mass of the clump is $190 d_2^2$ $M_\odot$. Second, the total CO flux in the rectangular area bounded by (α_{1950}, δ_{1950}) = ($19^h55^m15^s.3$, +32°45′50″) and ($19^h54^m43^s.5$, +32°52′32″) is $\iint T_A\,dv\,d\Omega = 6.4 \times 10^{-6}$ K km s^{-1}. If we use the ratio of H_2 column density to integrated CO J = 1–0 line intensity of $N_{H_2}/I_{CO} = 2.3 \times 10^{20}$ molecules cm^{-2} (K km s^{-1})$^{-1}$ (Strong et al. 1988), then the hydrogen mass of the clump is $130 d_2^2$ $M_\odot$, which agrees reasonably well with the

TABLE 1

PARAMETERS OF THE HV MOLECULAR OUTFLOW

Parameter	Estimated Value	Unit
Maximum velocity	~ 6	km s^{-1}
Size	~ 1 ($0.58d_2$)	arcmin (pc)
Age	$\sim 4.7 \times 10^4 d_2$	yr
Mass	$\sim 0.35 d_2^2$	$M_\odot$
Mass-loss rate	$\sim 7.4 \times 10^{-6} d_2$	$M_\odot$ yr^{-1}
Mechanical luminosity	$\sim 9 \times 10^{31} d_2$	ergs s^{-1}

previous estimate. We take $220 d_2^2\ M_\odot$ as the mass of the molecular clump.

In order to investigate the radial distribution of density in the clump, we compared the observed distribution of H_2 column density, which is assumed to be proportional to I_{CO}, with that predicted from a spherically symmetric cloud with a power-law radial distribution of density, i.e., $n_{H_2}(r) \propto r^{-k}$. The observed distribution is obtained by dividing the clump into concentric rings with a thickness of 25″ and by averaging the column density inside each ring. The predicted column density distributions are computed by integrating the density distribution along the line of sight and by convolving the result with a Gaussian beam of FWHM = 50″. Figure 3 compares the two for $k = 0$, 1, and 2. The column density distributions are normalized to have the same total mass. In Figure 3, the abscissa is the distance from the clump center normalized by 2.5. The density distribution with $k = 1$ seems to be consistent with the observed column density distribution. This power-law index, although uncertain because of our large beam width, is similar to $k = 1$–1.3 in other molecular clouds (Cernicharo, Bachiller, & Duvert 1985; Stüwe 1990) but smaller than $k = 1.6$ in dense cloud cores (Fuller & Myers 1992).

Toward the core of the molecular clump, we observed HCO^+ $J = 1$–0 line with negative results ($\Delta T_A = 0.03$ K), but we detected the CS $J = 2$–1 line. The peak antenna temperature of the detected CS line is 0.24 ± 0.02 K, and the integrated antenna temperature is 0.63 ± 0.05 K km s^{-1}. The CS

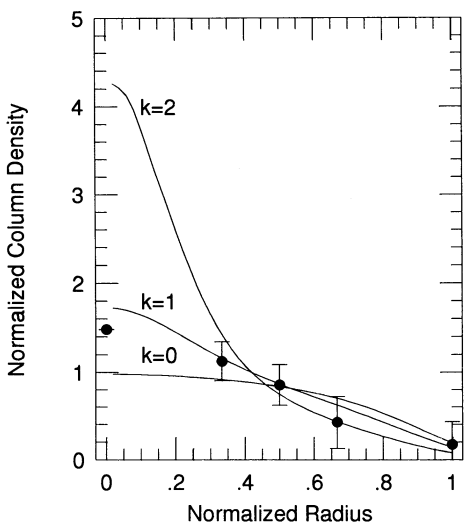

FIG. 3.—Observed H_2 column density distribution as a function of normalized distance from the clump center. The lines represent the expected column density distributions from a spherically symmetric cloud with $k = 0$, 1, and 2, where k is the power-law index of density distribution, i.e., $n_{H_2} \propto r^{-k}$. The column density distributions are normalized to have the same total mass.

$J = 2$–1 line originates from the densest part of the cloud core, where the molecular hydrogen density is typically between a few times 10^4 and 10^5 cm^{-3} and the kinetic temperature is typically between 10 and 20 K (Olano, Walmsley, & Wilson 1988; Blake, van Dishoeck, & Sargent 1992). A lower limit to the mass of the dense core may be estimated by assuming that the CS line is optically thin. If we assume that $T_{ex} = 15$ K, $[CS]/[H_2] = 1 \times 10^{-8}$ and that the dense core is much smaller than the main beam, then the mass of the dense core is greater than $1 d_2^2\ M_\odot$. It should be noted that this is a *lower* limit and that the mass of the dense core is probably much greater than $1 d_2^2\ M_\odot$.

We now consider the dynamical equilibrium of the molecular clump. For an isothermal spherical cloud with a density profile of $\rho(r) \propto r^{-k}$, the virial equilibrium requires (e.g., Spitzer 1978)

$$\frac{4\pi R^3 P_{ext}}{3Mc_{tot}^2} + \frac{(3-k)GM}{3(5-2k)Rc_{tot}^2} = 1\ , \qquad (1)$$

where R and M are, respectively, the radius and mass of the cloud, G is the gravitational constant, P_{ext} is the external pressure, and c_{tot} is the "effective sound speed" including the nonthermal contribution. In equation (1), the first and the second terms on the left-hand side are due to external pressure and self-gravity, respectively, whereas the term on the right-hand side is from internal pressure. The c_{tot} is related to the observed FWHM velocity Δv_{FWHM} by

$$c_{tot}^2 = \frac{\Delta v_{FWHM}^2}{8 \ln 2} + k_B T\left(\frac{1}{m_A} - \frac{1}{m_{obs}}\right), \qquad (2)$$

where k_B is the Boltzmann constant, T is the kinetic temperature, m_A (=2.33 amu for molecular gas with [He]/[H] = 0.1) is the mean mass per particle, and m_{obs} is the mass of the observed molecule (Myers 1983). If we use, in equation (2), the FWHM velocity $\Delta v_{FWHM} = 1.2$ km s^{-1} of the ^{13}CO line at the central position of the clump, we obtain $c_{tot} = 0.53$ km s^{-1}, with the contribution from thermal motion being negligible. (The optically thick ^{12}CO line is not adequate for estimating c_{tot} because it is saturated; neither is the CS line, for which we could not obtain a spectrum sensitive enough to derive the velocity width anyway, because it samples only the dense core.)

Using the power-law index $k = 1$, $M = 220 d_2^2\ M_\odot$, and $R = 1.5 d_2$ pc, equation (1) becomes

$$0.31 d_2 \left(\frac{P_{ext}/k_B}{4000\ \text{cm}^{-3}\ \text{K}}\right) + 0.50 d_2 = 1\ , \qquad (3)$$

where we normalized P_{ext} by a typical interstellar pressure (e.g., Kulkarni & Heiles 1987). The near equality between the internal pressure term and the sum of the self-gravity and external pressure terms in equation (3) implies that the clump is close to virial equilibrium.

4. THE CENTRAL SOURCE IRAS 19550+3248

4.1. *Morphology*

Located at the center of the bipolar outflow is the *IRAS* point source IRAS 19550+3248, which is almost certainly the young stellar object driving the molecular outflow. We obtained optical and near-infrared images of this region and detected an infrared source with nebulosity inside the 95% confidence ellipse of *IRAS* position. Figure 4 shows the I and K images of the source. In K band, the peak occurs at

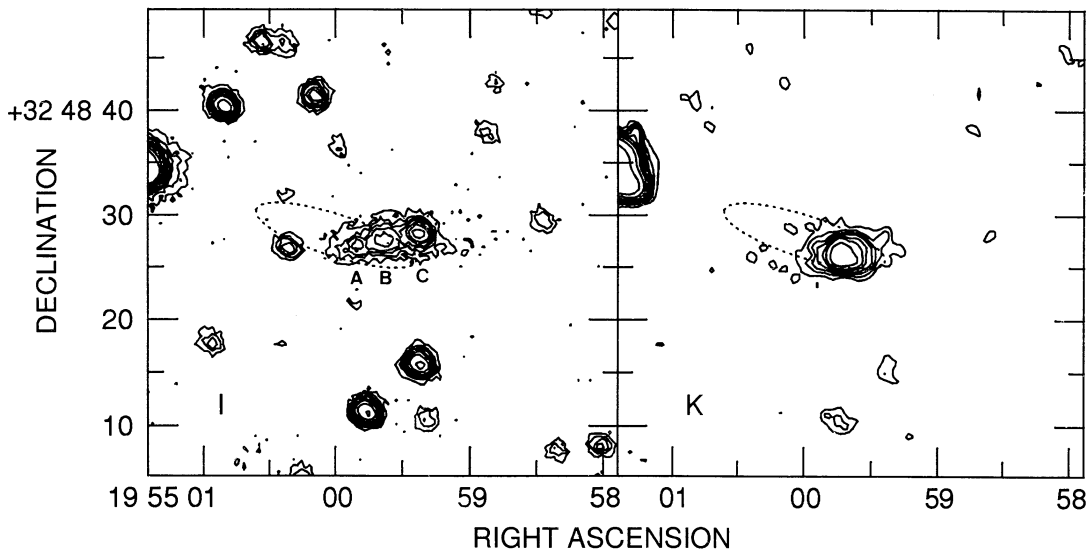

FIG. 4.—*I* and *K* band images of IRAS 19550+3248. The contour intervals are 1, 2, 3, 4, 6, 8, 12, 20, and 40 in an arbitrary unit. The dotted line represents the 95% confidence ellipse of *IRAS* position.

($19^h54^m59^s.70$, +32°48′26″.3). The coordinates were determined using the *Hubble Space Telescope* Guiding Star Catalog (GSC), and the positional error relative to the GSC position is 0″.2 (1 σ). Although the GSC has an estimated positional error of 0″.5, we found in this region a systematic difference of $\sim$2″.0 between the right ascensions of field stars given in the GSC and those given in the SAO catalog. We have not incorporated this systematic difference, and we quote 0″.5 as the positional uncertainty. In *K* band, the source extends $\sim$10″ ($=0.1d_2$ pc) along the east-west direction, roughly perpendicular to the bipolar axis. The weak extended emission toward the northwest, however, is likely to be contaminated by another star (see next paragraph).

In *I* band, we see three aligned peaks, A, B, and C (from east to west). The brightest (*I* magnitude of 16.67 $\pm$ 0.02), peak C, lying outside the 95% confidence ellipse of *IRAS* position, is located 4″.5 off the peak position in *K* band. The large positional shift suggests that peak C is *not* directly associated with IRAS 19550+3248. On the other hand, the a priori probability for a field star to be aligned with the other two peaks A and B might be very small. Furthermore, peak C has a color index of $V-I = 2.58 \pm 0.04$, which is considerably redder than the typical $\sim$1.5 value for other stars of similar magnitude in this field. We are not certain whether peak C bears any relation to IRAS 19550+3248. (Detailed photometric study of the stars in this field will be presented elsewhere; Koo & Lee 1993.) The other two peaks, A and B, are much fainter, with *I* magnitudes of 18.16 $\pm$ 0.05 and 17.48 $\pm$ 0.03, respectively. (They are not seen in *V* band, i.e., $V > 21.5$.) But they show profiles much more extended than that of peak C or of other stars of similar magnitude. Therefore, peaks A and B may be not stars but extended objects. Both peak A and peak B are shifted from the *K* band peak by 1″.5 ($0.015d_2$ pc), which is significantly greater than the relative positional uncertainty of 0″.4 between *I* and *K* images.

The two peaks A and B, separated by $\sim 0.024d_2$ pc, are located to the north of the *K* band peak, i.e., toward the blueshifted CO lobe. In nearby protostellar objects, a similar geometrical relationship has been found between the near-infrared emission and the bipolar molecular outflow. For example, in L1551 IRS 5, high-resolution imaging by Strom et al. (1985) and Hodapp et al. (1988) revealed an extended conical *H* and *K* emission opened toward the blueshifted lobe of the bipolar outflow. A detailed astrometric study has shown that the near-infrared and optical peaks are shifted systematically (with a shorter wavelength peak further apart) from the radio continuum peak, which is believed to be the true position of the young stellar object (Campbell et al. 1988). The near-infrared and optical emissions have been interpreted as the scattered stellar light from the inner surface of a thick disk surrounding the protostellar object. Hence, the near-infrared emission in Figure 4 is likely the scattered stellar light, and the protostar may be located slightly to the south of the *K* band peak.

4.2. *Spectral Flux Density Distribution*

The photometry has been done in *R*, *I*, *H*, and *K* bands, and the results are given in Table 2, together with the *IRAS* fluxes. In Table 2, the *R* and *I* fluxes are obtained excluding peak C. Figure 5 shows the spectral flux density distribution. The luminosity integrated over the observed wavelength range (0.64–100 μm) with a linear interpolation is $100d_2^2\ L_\odot$. The long-wavelength bolometric correction is made by assuming a blackbody curve with its peak at 100 μm (see Myers et al. 1987, hereafter MET87) and is equal to 47 $L_\odot$. Hence, the bolometric luminosity of IRAS 19550+3248 is $150d_2^2\ L_\odot$. Similar to other HV molecular outflow sources, the radiation force of IRAS 19550+3248 is not sufficient (by a factor of $10d_2^{-1}$) to drive the

TABLE 2

PHOTOMETRY OF IRAS 19550+3248

Band	Flux Density (Jy)
R (0.64 μm)	$8.3\ (0.5) \times 10^{-5}$
I (0.79 μm)	$4.0\ (0.14) \times 10^{-4}$
H (1.65 μm)	$9.3\ (0.9) \times 10^{-3}$
K (2.16 μm)	$1.47\ (0.15) \times 10^{-2}$
12 μm	<0.29
25 μm	1.76 (0.11)
60 μm	10.2 (1.0)
100 μm	22.1 (2.2)

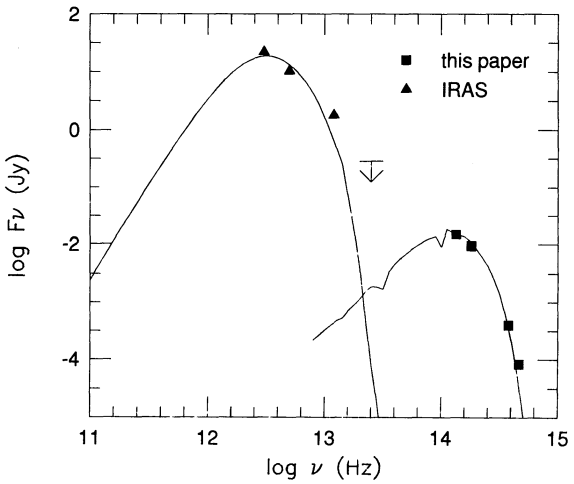

FIG. 5.—Spectral flux density distribution of IRAS 19550+3248. The line at near-infrared represents the attenuated blackbody radiation, while the line at far-infrared represents the reprocessed emission from the dust envelope (see § 4.2).

molecular outflow. It is unknown whether IRAS 19550+3248 has a neutral stellar wind, as do some other protostellar objects (see references in Koo 1993).

The spectral index n between the near-infrared and mid-infrared, defined by

$$n \equiv \frac{d \log (\nu F_\nu)}{d \log \nu}, \tag{4}$$

may be used to classify the nature of an infrared source (Adams, Lada, & Shu 1987; Lada 1991). For IRAS 19550+3248, the spectral index between 2 and 25 μm is $n = -0.93$. This steep spectral index is typical for a protostar deeply embedded in a molecular cloud core (MET87).

The spectral flux density distribution in Figure 5 is fitted with a simple model where a point source is surrounded by a dust envelope. The central point source is assumed to emit a blackbody radiation corresponding to temperature T_*. Most of this radiation is absorbed by the dust envelope and reemitted in the far-infrared. The escaping stellar emission appears in the near-infrared and optical wavelength. A detailed explanation of this model is given in MET87, and here we give only a brief summary. By comparing the observed H and K flux densities with the attenuated blackbody emission, we obtain the temperature of the central protostar $T_* = 8300$ K and the visual extinction of the dust envelope $A_V = 14$ mag. This visual extinction is considerably smaller than the $\sim$24 mag expected from the correlation between the spectral index n and A_V found in MET87. As shown in Figure 5, the attenuated blackbody emission fits the observed K, H, I, and R flux densities very well.

The far-infrared portion of the spectrum of IRAS 19550+3248 has been fitted by the emission from a dust envelope with inner radius r_1 and outer radius $r_2 = 2 \times 10^{17}$ cm. The temperature distribution inside the dust shell is given by $T(r) = T_1(r/r_1)^{-0.4}$. The density distribution is given by $n_{H_2} = n_1(r/r_1)^{-p}$ with a mean density of $\langle n_{H_2} \rangle = 3 \times 10^4$ cm^{-3}. Once the power-law index p is given, the inner radius r_1 and the density n_1 are determined by A_V, r_2, and $\langle n_{H_2} \rangle$. As can be seen from the results of MET87, the flux density distribution is rather insensitive to p as it varies from 1.25 and 2.0. The solid curve in Figure 5 is for $p = 1.5$ ($r_1 = 2.0 \times 10^{16}$ cm) and $T_1 = 60$ K, and it fits 25, 60, and 100 μm flux densities reasonably well. The derived parameters of IRAS 19550+3248 are summarized in Table 3.

TABLE 3

PARAMETERS OF IRAS 19550+3248

Parameter	Estimated Value
$(\alpha_{1950}, \delta_{1950})$	($19^h54^m59^s.70$, $+32°48'26''.3$)
Size	$\leq 10''$ ($0.1 d_2$ pc)
Bolometric luminosity	$\sim 150 d_2^2\ L_\odot$
Spectral index between 2 and 25 μm	-0.93
Visual extinction[a]	14 mag
Stellar temperature[a]	8300 K

[a] See text § 4.2.

5. DISCUSSION

5.1. *Filamentary Molecular Cloud*

The molecular clump where IRAS 19550+3248 has formed is connected to a long filamentary molecular cloud, called "cloud A" by KYHL (see Fig. 2). Detailed study of this molecular cloud might be essential to understanding the formation of IRAS 19550+3248. Here we consider some of the cloud's overall properties. Cloud A extends $\ell \sim 40 d_2$ pc and has a mass of $M_c \sim 2100 d_2^2\ M_\odot$ (KYHL). Figure 2 shows that the structure of cloud A is complex: there are dense clumps, thin filaments, and holes. The morphology of the cloud suggests that it is not strongly self-gravitating. The relative significance of self-gravity may be appraised by the dimensionless parameter $P/G\sigma_c^2$, where σ_c is the cloud surface mass density and P is either external or internal pressure (e.g., Elmegreen 1991). The mean surface density of cloud A is $\sigma_c \sim 13\ M_\odot$ pc^{-2}. The corresponding gravity "pressure" is $G\sigma_c^2 \sim 5 \times 10^{-13}$ dyn cm^{-2}. For a typical interstellar pressure (e.g., $P_{ext}/k \sim 4000$ cm^{-3} K) therefore, $P_{ext}/G\sigma_c^2 \sim 1$. For comparison, the ratio is $\sim$0.006 for a typical giant molecular cloud in our Galaxy (Solomon et al. 1987). In order to compare with the internal pressure, we use a mean density of $\bar{\rho} = \sigma_c/D \sim 2.2 \times 10^{-22} d_2^{-1}$ g cm^{-3}, where $D = 4 d_2$ pc is a characteristic thickness obtained from the geometrical area $A_g = 160 d_2^2$ pc^2 divided by the length ℓ. If we use the effective sound speed $c_{tot} = 0.53$ km s^{-1} in § 3.2, the ratio is $\bar{\rho} c_{tot}^2/G\sigma_c^2 \sim 1 d_2^{-1}$. Hence, the self-gravity is *not* particularly dominant compared to either external or internal pressure, for cloud A.

It is the supersonic motion of clumps that dominates the dynamics of the cloud. The velocity structure of the cloud along the right ascension is shown in Figure 6, which is obtained by squeezing all the CO emission between $\delta = +32°38'$ and $33°04'$. Several points are to be made from Figure 6. First, most molecular gas moves at $\bar{v}_{LSR} = +11.3$ km s^{-1}. (The average velocity $\bar{v}_{LSR}$ is a mean, weighted by peak antenna temperatures, i.e., $\bar{v}_{LSR} \equiv (\Sigma T_{peak} v_{peak})/(\Sigma T_{peak})$, where T_{peak} and v_{peak} are the antenna temperature and the LSR velocity of the peak CO emission for a given pixel, respectively, and the summation is over all pixels with $T_{peak} > 0.5$ K in cloud A.) Second, the velocity dispersion among clumps is large. The observed velocity dispersion of cloud A—defined by $\sigma_v^2 \equiv [\Sigma T_{peak}(v_{peak} - \bar{v}_{LSR})^2]/(\Sigma T_{peak})$, where, again, the summation is over all pixels with $T_{peak} > 0.5$ in cloud A—is $\sigma_v = 2.2$ km s^{-1}. The ratio of the ram pressure to the gravity pressure is $\bar{\rho}\sigma_v^2/G\sigma_c^2 \sim 20 d_2^{-1}$. In particular, note that there are clumps

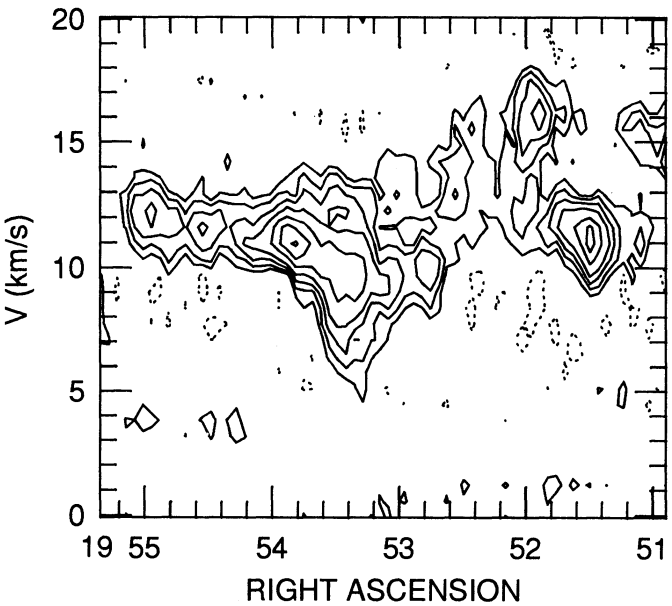

FIG. 6.—Right ascension vs. velocity diagram of cloud A, in Fig. 2. The ^{12}CO emission has been squeezed in declination ($\delta = +32°38'$ to $+33°04'$) to show the variation of an average antenna temperature $\bar{T}_A$ along right ascension. The contour intervals (in K) and $\bar{T}_A = -0.06, 0.06, 0.12, 0.2, 0.3, 0.5, 0.7$, and 0.9. Dotted lines represent negative antenna temperatures. (See also Figs. 5 and 6 of KYHL.)

moving at either $v_{LSR} = +7$ or $+16$ km s^{-1} (see also Figs. 5 and 6 of KYHL). For these clumps, the ratio is $\sim 100 d_2^{-1}$. Hence, the clumps in cloud A are not gravitationally bound to form a large filamentary cloud. Also, the large ram pressure ($\bar{\rho}\sigma_v^2/k_B = 1$–$4 \times 10^5$ K cm^{-3}) and the complex morphology suggest that cloud A is probably not confined by an external pressure.

A possible explanation for the physically associated, but not confined either by gravity or by an external pressure, clumps in cloud A is that they are products of a collision between two clouds. Collision between two clouds has been studied by several authors (e.g., Hausman 1981; Gilden 1984; Lattanzio et al. 1985; Habe & Ohta 1992). The final outcome of a cloud-cloud collision depends on the cloud densities, the cloud sizes, the relative velocity of collision, and the impact parameter. It also depends on the initial shapes of the colliding clouds. For spherically symmetric clouds, it has been shown that non–head-on collisions and large relative velocities tend to disrupt clouds (Hausman 1981; Lattanzio et al. 1985). Although detailed modeling is required, it seems to be quite possible that highly irregular clouds such as cloud A can be produced from disruptive collisions. The characteristic dispersal timescale for cloud A is $t_c \equiv (A_g)^{1/2}/\sigma_v \sim 6 \times 10^6$ yr. It is worth mentioning that the western portion of cloud A and cloud B form an almost closed loop (see Fig. 2) and have a systematic velocity gradient of $\sim 0.2 d_2^{-1}$ km s^{-1} pc^{-1} (see KYHL). The loop structure and the systematic velocity gradient may be interpreted as an expanding ring, with its line of nodes crossing from northeast to southwest. The characteristic timescale for the expanding motion is almost identical to t_c. If we consider this expanding loop to be produced by a collision, then a picture emerges in which a small dense cloud penetrates into a relatively large diffuse cloud (e.g., see Habe & Ohta 1992). Under this picture, the cometary morphology of the eastern portion of cloud A suggests that the molecular clump where IRAS 19550+3248 has formed is the small cloud that has penetrated the large cloud.

5.2. *Formation of* IRAS 19550+3248

We checked the positions of *IRAS* point sources in this region (*IRAS* Point Source Catalog, Version 2 1988). There are eight sources seen against cloud A. None of them has a spectral energy distribution corresponding to "infrared protostars" (class I sources; Lada 1991), except IRAS 19550+3248. The clump where IRAS 19550+3248 has formed (hereafter "clump IRS") seems to be the only region in cloud A where a luminous protostar is deeply embedded. (The minimum luminosity detectable by *IRAS* is $23 d_2^2\ L_\odot$ for $n = -0.5$; see MET87.) What made clump IRS, located at the tip of a large filamentary molecular cloud, separate to form a star? Based on our discussion at the end of § 5.1, we speculate that clump IRS is a small compressed cloud that has penetrated a large diffuse cloud. For such collisions, Habe & Ohta (1992) have shown that the small cloud, initially at stable hydrostatic equilibrium, develops a dense clump which may become gravitationally unstable. If our speculative picture is correct, then we have a remarkable example of star formation due to a cloud-cloud collision.

There has been a claim that the ratio of the luminosity of a young stellar object to the mass of the core of the parental isolated globule may be used to characterize the different star formation mechanism in globules (Sugitani et al. 1989). The ratios in a sample of bright-rimmed globules, 3–13 $L_\odot/M_\odot$, turned out to be higher than those of isolated dark globules with similar masses, 0.03–0.3 $L_\odot/M_\odot$, which led Sugitani et al. to suggest that the young stellar objects in bright-rimmed globules, presumably formed by ionization-shock implosion, are more luminous and perhaps more massive than those formed in isolated quiescent globules. For IRAS 19550+3248, the ratio lies between 1 and 200, depending on how we define the core. (For comparison with the result of Sugitani et al., we used the mass of the molecular hydrogen.) The ratio is most likely 5–10, if we define the core as the area to be seen in ^{13}CO $J = 1$–0 line. The large ratio may be more evidence for the shock-induced formation of IRAS 19550+3248.

6. SUMMARY

We have performed radio, near-infrared, and optical observations of IRAS 19550+3248, a protostellar object deeply embedded in a dense molecular core. The distance to the source is uncertain, and we used the normalized distance $d_2 = d/(2$ kpc) in this paper. The molecular clump where IRAS 19550+3248 has formed is located at the tip of a long filamentary molecular cloud. There is no evidence of other luminous protostars in the cloud. The molecular cloud has a complex structure composed of clumps, filaments, and holes. The clumps are not confined by gravity and nor probably by an external pressure. We suggest that the complex structure is possibly the result of a collision between a small dense cloud and a large diffuse cloud. An expanding looplike structure may have been produced by the collision. The characteristic timescale for the collision event is $t_c \sim 6 \times 10^6$ yr. We further speculate that IRAS 19550+3248 has formed within the small shock-compressed cloud, which has penetrated the large cloud. We summarize our main results below:

1. We have detected a bipolar CO outflow around IRAS 19550+3248. The mechanical luminosity of the HV molecular

outflow is $\sim 9 \times 10^{31} d_2$ ergs s^{-1}, and its dynamical age is $\sim 5 \times 10^4 d_2$ yr. Other physical parameters of the molecular outflow are given in Table 1.

2. We have detected CS $J = 2$–1 emission toward the molecular clump where IRAS 19550+3248 is embedded. A *lower* limit on the mass of the dense core is $1 d_2^2 M_\odot$. By analyzing the physical properties of the clump, we found that the clump is close to virial equilibrium.

3. In K band, IRAS 19550+3248 shows an extended emission along the east-west direction. Images in I and R bands show the source is composed of two extended weak peaks shifted symmetrically from the peak position in K band. The two peaks, separated by $\sim 0.024 d_2$ pc, are located at the north of the K band peak, i.e., toward the blueshifted CO lobe. This geometrical relationship between the bipolar flow and the near-infrared nebulosity is similar to that other nearby protostellar objects and suggests that the near-infrared emission is likely the scattered stellar light.

4. IRAS 19550+3248 has a steep spectral index between 2 and 25 μm, $n = -0.93$, which is typical for a protostar deeply embedded in a molecular cloud core. The bolometric luminosity is $150 d_2^2 L_\odot$ and is not sufficient to drive the molecular outflow. The observed spectral flux density distribution is explained by a simple model where a point source emitting blackbody radiation is surrounded by a dust envelope. The physical parameters of IRAS 19550+3248 are given in Table 3.

5. The ratio of the luminosity of IRAS 19550+3248 to the mass of the parental molecular clump is comparable to such ratios found in bright-rimmed globules. The large ratio may be more evidence for the shock-induced formation of IRAS 19550+3248.

We wish to thank S. S. Hong, P. C. Myers, and W. T. Reach for their helpful comments. B.-C. K. and G. A. F. acknowledge the support of Center for Astrophysics Postdoctoral Fellowships. G. A. F. also acknowledges the support of a National Radio Astronomy Observatory Jansky Fellowship. This work has been supported in part by the Korean Astronomical Observatory Research Fund (B.-C. K.).

REFERENCES

Adams, F. C., Lada, C. J., & Shu, F. H. 1987, ApJ, 312, 788
Blaauw, A. 1991, in The Physics of Star Formation and Early Stellar Evolution, ed. C. J. Lada & N. D. Kylafis (Dordrecht: Reidel), 125
Blake, G. A., van Dishoeck, E. F., & Sargent, A. I. 1992, ApJ, 391, L99
Campbell, B., Persson, S. E., Strom, S. E., & Grasdalen, G. L. 1988, AJ, 95, 1173
Cernicharo, J., Bachiller, R., & Duvert, G. 1985, A&A, 149, 273
Elmegreen, B. G. 1991, in The Physics of Star Formation and Early Stellar Evolution, ed. C. J. Lada & N. D. Kylafis (Dordrecht: Reidel), 35
Fuller, G. A., & Myers, P. C. 1992, ApJ, 384, 523
Gilden, D. L. 1984, ApJ, 279, 335
Gomez de Castro, A. I., & Pudritz, R. E. 1992, ApJ, 395, 501
Habe, A., & Ohta, K. 1992, PASJ, 44, 203
Hausman, M. A. 1981, ApJ, 245, 72
Hodapp, K.-W., Capps, R. W., Strom, S. E., Salas, L., & Grasdalen, G. 1988, ApJ, 335, 814
IRAS Point Source Catalog, Version 2. 1988, Joint *IRAS* Science Working Group (Washington, D.C.: GPO)
Koo, B.-C. 1993, in 2d North-Asian Regional Meeting on Recent Development in Millimeter-Wave and Infrared Astronomy, ed. S. H. Cho & H. S. Chung (Daejon: Korean Astronomy Observatory), 130
Koo, B.-C., & Lee, M. G. 1993, in preparation
Koo, B.-C., Yun, M.-S., Ho, P. T. P., & Lee, Y. 1993, ApJ, 417, 196 (KYHL)
Kulkarni, S. R., & Heiles, C. 1987, in Interstellar Processes, ed. D. J. Hollenbach & H. A. Thronson (Dordrecht: Reidel), 87
Lada, C. J. 1991, in The Physics of Star Formation and Early Stellar Evolution, ed. C. J. Lada & N. D. Kylafis (Dordrecht: Reidel), 329
Lada, C. J., Blitz, L., & Elmegreen, B. G. 1978, in Protostars and Planets, ed. T. Gehrels (Tucson: Univ. Arizona Press), 341
Landolt, A. U. 1992, AJ, 104, 340
Lattanzio, J. C., Monaghan, J. J., Pongracic, H., & Schwarz, M. P. 1985, MNRAS, 215, 125
Loren, R. B. 1976, ApJ, 209, 466
Mouschovias, T. C. 1987, in Physical Processes in Interstellar Clouds, ed. G. E. Morfill & M. Scholer (Dordrecht: Reidel), 453
Mouschovias, T. C., & Morton, S. A. 1992a, ApJ, 390, 144
———. 1992b, ApJ, 390, 166
Myers, P. C. 1983, ApJ, 270, 105
Myers, P. C., Fuller, G. A., Mathieu, R. D., Beichman, C. A., Benson, P. J., Schild, R. E., & Emerson, J. P. 1987, ApJ, 319, 340 (MET87)
Olano, C. A., Walmsley, C. M., & Wilson, T. L. 1988, A&A, 196, 194
Schechtor, P. L., Mateo, M., & Saha, A. 1993, preprint
Shu, F. H., Adams, F. C., & Lizano, S. 1987, ARAA, 25, 23
Solomon, P. M., Rivolo, A. R., Barrett, J., & Yahil, A. 1987, ApJ, 319, 730
Spitzer, L. I. 1978, Physical Processes in the Interstellar Medium (New York: Wiley)
Strom, S. E., Strom, K. M., Grasdalen, G. L., Capps, R. W., & Thompson, D. 1985, AJ, 90, 2575
Strong, A. W., et al. 1988, A&A, 207, 1
Stüwe, J. A. 1990, A&A, 237, 178
Sugitani, K., Fukui, Y., Mizuno, A., & Ohashi, N. 1989, ApJ, 342, L87
Zhou, S., Evans, N. J., II, Butner, H. M., Kutner, M. C., Leung, C. M., & Mundy, L. G. 1990, ApJ, 363, 168